Significance of Al doping for antiferromagnetic AFII ordering in $YBa_2Cu_{3-x}Al_xO_{6+\delta}$ materials: A single-crystal neutron-diffraction study

E. Brecht, W.W. Schmahl, and H. Fuess
Fachbereich Materialwissenschaft-Strukturforschung, Technische Hochschule Darmstadt, Petersenstrasse 20, D-64287 Darmstadt, Germany

H. Casalta, P. Schleger, B. Lebech, and N. H. Andersen
Risø National Laboratory, Department of Solid State Physics, DK-4000 Roskilde, Denmark

Th. Wolf
Forschungszentrum Karlsruhe, Institut für Technische Physik, P.O. Box 3640, D-76021 Karlsruhe, Germany
(Received 22 March 1995)

Aluminum-doped, oxygen-deficient $YBa_2Cu_{3-x}Al_xO_{6+\delta}$ single crystals with different Al contents x ($0 \leq x \leq 0.19$) and O contents ($0.18 \leq \delta \leq 0.36$) were studied by magnetic neutron diffraction. All of the Al-doped single crystals show two magnetic transitions, the first between the paramagnetic state and the AFI phase, and a second transition at low temperatures between the AFI and the AFII phase. The Néel temperature T_N of the antiferromagnetic AFI phase is found to be insensitive to the Al content x as well as the O content $6+\delta$ in the x-δ region investigated so far. In a limited temperature interval the order parameter shows the components of both the AFI and AFII phases indicating competing interactions. For some crystals a complete reordering to the AFII phase at 4.2 K can be observed. Although the antiferromagnetic ordering pattern is different for the AFI and AFII phase, the ordered moments on the Cu sites are within the experimental error ($\langle S\rangle_{Cu(2)} \approx 0.56\mu_B$, $\langle S\rangle_{Cu(1)} \approx 0\mu_B$) identical in the two phases. Comparison of Al-doped crystals with pure crystals of the same oxygen content shows that the presence of excess oxygen only ($\delta>0$) is not sufficient to obtain the AFII ordering at low temperatures. Instead, the AFII ordering is triggered by the creation of the local magnetic moments in Cu–O–Al chain fragments.

I. INTRODUCTION

The study of antiferromagnetic order of pure and cation-doped $YBa_2Cu_3O_{6+\delta}$ and related compounds is a field of considerable interest, since the underlying mechanism of the electronic and magnetic properties even of the nonsuperconducting state is still not fully understood. Indication of antiferromagnetic long-range order was first observed by Nishida *et al.*[1] using muon spin relaxation. The antiferromagnetic structure AFI was determined by Tranquada *et al.*[2] by magnetic neutron scattering on polycrystalline samples. In this phase the spins on the Cu(2) sites alternate antiferromagnetically within the CuO_2 planes and along the tetragonal **c** axis [see Fig. 1(a)]. The average ordered moment on the Cu(2) lattice site was found to be about 0.52 μ_B with the spins oriented perpendicular to the **c** axis.[3] No ordered magnetic moment was found on the Cu(1) sites in the oxygen-deficient layer. The ordered magnetic moment as well as the Néel temperature T_N of this phase were reported to depend on the oxygen content.[4–7] For $0 < \delta < 0.2$ the Néel temperature is above 400 K and almost independent of δ, while T_N decreases rapidly with increasing oxygen content for $\delta > 0.3$. Magnetic neutron scattering studies were reported for reduced polycrystalline material[4,6–8] as well as for undoped YBaCuO single crystals,[6–9] which all show the AFI phase with approximately the same values for T_N and for the average magnetic moment for a given O content. Kadowaki *et al.*[10] were the first to report an antiferromagnetic reordering to a second magnetic phase (AFII) at low temperature with a transition temperature T_2 of about 40 K in an $YBa_2Cu_3O_{6.35}$ single crystal. This antiferromagnetic low-temperature phase is associated with the presence of Cu^{2+} moments in the oxygen-deficient Cu(1) chain layer which leads to a doubling of the magnetic unit cell along **c** [see Fig. 1(b)]. Very recently the AFII phase was also reported by Shamoto *et al.*[3] in a sample with a T_2 of about 15 K. The AFII phase is also known from neutron-diffraction studies on the $Nd_{1+y}Ba_{2-y}Cu_3O_{6+\delta}$ system.[11,12] However, this system may show a different magnetic behavior compared to the Y system, because Nd^{3+} is a magnetic rare earth ion, which, moreover, substitutes on the Ba sites.[13–16]

Therefore, except for the two observations[3,10] mentioned above, the AFII phase has, to our knowledge, not been observed in either polycrystalline or single-crystal material of the undoped Y compound. Recent magnetic neutron-diffraction measurements on very pure, high quality single crystals by Casalta *et al.*,[17] which were prepared in zirconia crucibles, did not show any AFII phase down to the experimental limit of 2 K, either.

Extensive studies have been carried out in order to understand the influence of the M^{3+} cations on both the Cu(1) "chain" and Cu(2) "plane" lattice sites on the

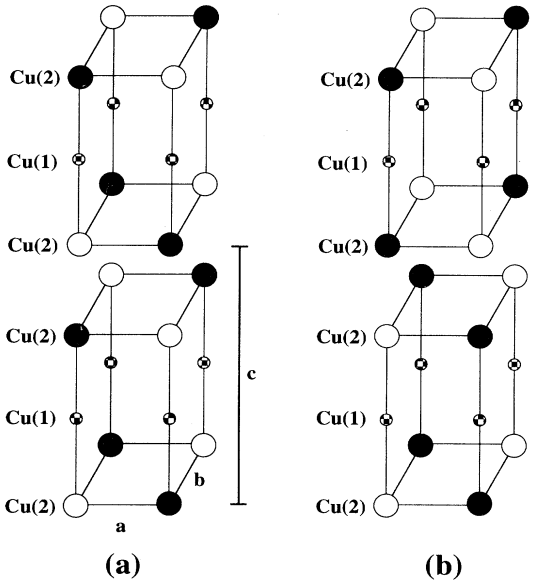

FIG. 1. Structure of the antiferromagnetic (a) AFI and (b) AFII phase. The moment direction for both phases is within the *ab* plane. Filled and open Cu(2) atoms have oppositely directed ordered moments. The ordered moments on the Cu(1) atoms are insignificant.

structural, superconducting, and magnetic properties of $YBa_2Cu_{3-x}M_xO_{6+\delta}$.[18–24] It was found that Ni^{2+} and Zn^{2+} substitute mainly on the Cu(2) sites,[18] dramatically affecting the superconducting transition temperature T_c, while M =Co^{3+}, Fe^{3+}, and Al^{3+} substitute predominantly on the Cu(1) lattice sites.[18] The latter substitution induces a structural transition from orthorhombic to tetragonal symmetry at about $x = 0.09$,[19,20] and results in a quite moderate decrease of the superconducting properties with increasing dopant content.[24] It should be noted that the results for Al-doped compounds are somewhat easier to interpret compared to the Fe- and Co-doped systems, since a certain amount of Fe and Co also substitutes on the Cu(2) sites. This fact was found by Mössbauer investigations on Fe-doped ceramics, where the Fe amount on the Cu(2) sites can be increased during reduction at high temperatures.[25] Substitution of Co on Cu(2) sites was also observed by neutron powder diffraction studies on Co-doped material.[26] Another remarkable feature of doped samples is the fact that reduction at high temperatures followed by a subsequent oxidation at low temperatures results in a structural change from tetragonal to orthorhombic symmetry, which has been reported for the Fe-doped[25,27,28] and Co-doped[29] systems. For the Al-doped system similar results have been found.[30] This observation is interpreted as due to a clustering of the defect ions on Cu(1) lattice sites during the reduction process due to the higher coordination of the dopant.

Magnetic neutron scattering investigations on Co-doped[26,31,32] and Fe-doped[33–35] ceramic samples show that for a low level of substitution the transition to the AFII phase is found at low temperatures. However, the AFII phase becomes stable in a wider temperature range for high substitution levels of the formally nonmagnetic Cu^+ by these magnetic ions.

Parallel to neutron-diffraction studies, the magnetic order has been studied in detail by Cu-NQR.[36] In the case of AFII ordering, the dipolar and magnetic hyperfine field induced by the magnetic Cu(2) ions lead to a splitting of the NQR line of Cu(1) by about 0.2 T. In the AFI structure this field disappears at the Cu(1) site by symmetry. From these investigations it was observed that most Y-Ba-Cu-O samples show the AFI state down to $T = 1.1$ K independent of the oxygen content $6+\delta$ across the entire width of the antiferromagnetic phase space. It has also been reported[36] that the AFII structure can be induced by a small doping with a trivalent ion on the Cu(1) sites like Fe, Al, Ga, whereas no field was observed from samples doped with the divalent Zn or Ni.[36]

Another sensitive probe for the study of the magnetism in these compounds is the Mössbauer experiment, which has been applied to Fe-doped ceramics.[35,37,38] In these experiments the AFI↔AFII reordering is also observed at low temperatures for low Fe concentration, whereas a higher doping level is found to stabilize the AFII structure.

In this work we present a neutron-diffraction study on $YBa_2Cu_{3-x}Al_xO_{6+\delta}$ single crystals with different Al and O contents. Our work is motivated by the question of whether and how the nonmagnetic Al ions influence the magnetic properties of the Y-Ba-Cu-O system. This is also an important problem of materials preparation since Al_2O_3 is used as a crucible material in many crystal growth experiments for $YBa_2Cu_3O_{6+\delta}$, where doping by Al cannot be avoided.

II. EXPERIMENTAL DETAILS

A. Sample preparation

The Al-doped single crystals were grown from a BaO/CuO flux in Al_2O_3 crucibles using different oxygen partial pressures and cooling rates. Table I lists the relevant growth parameters. Further details of the growth procedure are given elsewhere.[39] Al doping of the crystals was a consequence of crucible corrosion. The rate of crucible corrosion was found to be controlled by the growth temperature, cooling rate, and by the oxygen partial pressure during growth. The Al content was determined by single-crystal neutron diffraction (see below). EDX microprobe studies of typical crystals did not indicate any lateral changes of the Al content. The as-

TABLE I. Relevant growth parameters of the crystals from different batches.

Batch	Crucible	Ba source	Cooling rate	Atmosphere
WAX1	Al_2O_3	$BaCO_3$	0.3 K/h	1 bar O_2
WAX5	Al_2O_3	$BaCO_3$	0.18 K/h	0.12 bar O_2
WAX17	Al_2O_3	BaO_2	0.3 K/h	1 bar O_2
WAX28	ZrO_2/Y	BaO	0.4 K/h, 0.3 K/h	Air
TWOX197	Al_2O_3	BaO	0.5K/h, 0.3K/h	Air

grown crystals were annealed in flowing oxygen between 873 K and 673 K during 500–660 h. The structural perfection of the crystals was analyzed by high-resolution x-ray–diffraction measurements. The full width at half maximum (FWHM) of the rocking curve of the (005) peak was always far below 0.1°, which indicates a small mosaic spread of these crystals. Another very sensitive probe for determinination of the crystalline quality is ion channeling experiments, which were performed on a typical crystal with an Al content $x = 0.19$ using 2 MeV He^+ ions at a backscattering angle of 165°. We obtained a minimum yield χ_{min} of 3.3% at the Ba edge. This also demonstrates the high crystalline quality of these Al-doped crystals, compared to undoped crystals of high quality, where a χ_{min} between 2 and 3% is observed.[40] Likewise, the width of the superconducting transition of the oxidized crystals as measured by ac susceptibility did not indicate structural or chemical inhomogeneities.

The oxygenated crystals were reduced under different conditions and the oxygen contents of the different crystals are summarized in Table II. WAX17-1B ($x = 0.19$), WAX1-1A ($x = 0.14$), WAX5-1 ($x = 0.07$), TWOX197-1 ($x = 0.06$) were deoxygenated at 923 K under the same conditions as in Ref. 17 using a gas volumetric technique.[41,42] Under these conditions Casalta *et al.*[17] attained an oxygen content of δ=0.1 for the undoped crystal. WAX17-1A ($x = 0.19$) was reduced at 973 K for 48 h in a N_2 gas flow. The purity of the nitrogen was 99.8%. The samples WAX17-1C ($x = 0.19$) and WAX1-1B ($x = 0.10$) were reduced at 1044 K for 64 h in a He flow (1 bar) with repeated pumping sequences in order to completely change the atmosphere in the furnace. Based on the purity of the He gas the oxygen partial pressure was lower than 10^{-5} bar during the reduction in order to keep the oxygen content of these crystals as low as possible. One crystal, WAX28-5 ($x = 0.0$), was grown in a ZrO_2/Y_2O_3 (yttria stabilized zirconia) crucible and therefore contains Al only in ppm traces. This crystal was reduced in the temperature range between 873 K and 773 K. To establish an oxygen content of δ=0.25, which is comparable to the oxygen content of the Al-doped crystals, the oxygen partial pressure was adjusted with temperature, according to the $T - p(O_2)$-δ phase diagram in Ref. 43.

TABLE II. Name of the sample batch, the superconducting transition temperature T_c^{mid} in the fully oxidized state, reduction temperature T_R, Al content x and O content δ in the basal plane, Néel temperature T_N, and onset temperature of the AFII phase T_2.

Sample	T_c^{mid}	T_R (K)	x	δ	T_N (K)	T_2 (K)
WAX17-1A	59(1)	973	0.19(2)	0.36(3)	412(1)	18(1)
WAX17-1B	59(1)	923	0.19(2)	0.28(3)	407(1)	17(1)
WAX17-1C	59(1)	1044	0.19(3)	0.25(3)	408(1)	13(1)
WAX1-1A	69(1)	923	0.14(3)	0.25(3)	411(1)	8(1)
WAX1-1B	69(1)	1044	0.10(3)	0.21(3)	404(1)	4(1)
WAX5-1A	79(1)	923	0.07(2)	0.14(3)	411(1)	7(1)
TWOX197	81(1)	923	0.06(2)	0.18(3)	403(1)	12(1)
WAX28-5[a]	89(1)	923	0*	0.23(2)	334(1)	< 2

[a]Crystal grown in ZrO_2/Y_2O_3 crucible.

B. Neutron diffraction

Nonpolarized magnetic neutron-diffraction experiments were performed on the TAS1 triple-axis spectrometer at Risø National Laboratory, Denmark (RNL) using incident neutrons of energy 13.7 meV (λ=2.42 Å) selected by a graphite monochromator. Contributions of higher order neutrons were minimized by a pyrolytic graphite filter. The collimation between monochromator and sample was 30', between sample and detector a collimation of 19' was employed. Most of the measurements were performed without analyzer crystal in order to relax the exit collimation. The samples were mounted on an aluminum rod and placed inside an aluminum can filled with He exchange gas. For most of the work a standard ^{4}He cryostat was used for temperatures between 2 K and 300 K. For measurements above room temperature the sample was mounted in a furnace can, which was filled with He gas to avoid oxygen takeup during heating. All the scans were performed in the (*hhl*) scattering plane. The sizes of the single crystals used for neutron-diffraction studies were typically $3 \times 3 \times 0.5$ mm^3.

In order to characterize the single crystals structurally and to determine the Al and O contents, complete nuclear Bragg scattering sets were collected by use of the TAS2 four-circle neutron diffractometer with incident neutrons of wavelength λ=1.047 Å. The structural parameters determined from the four-circle data were used in the subsequent analysis of the magnetic data.

III. RESULTS

A. Nuclear structure

The data collection on the four-circle diffractometer TAS2 was performed in the $\theta - 2\theta$ mode. We measured half a sphere of nuclear Bragg reflections up to $\sin\theta/\lambda = 0.67$ Å^{-1}. Typically 1052 reflections were measured leading to about 192 independent observations. Analysis of the nuclear structural data was performed by use of the SHELX76 (Ref. 44) refinement program. The R factors obtained in the refinement were about 2%. Details of the results are given elsewhere.[45] For the single crystal described here in most detail (WAX17-1B) the results can be summarized as follows: Al is found to occupy only the Cu(1) lattice site; within the standard deviation no Al enters the Cu(2) site. The apical oxygen is not fully occupied but shows a small deficiency of about 6%. Since this single crystal was reduced under the same conditions as the undoped high-purity crystal used by Casalta *et al.*,[17] the oxygen content found in the basal plane can be directly compared to the undoped system. For the Al-doped crystal with $x = 0.19(2)$ an oxygen content $\delta = 0.28(2)$ is obtained, while $\delta = 0.10$ in the Al-free material reduced under the same conditions. This clearly shows that aluminum pins a significant amount of residual oxygen in the chain layer. The refined contents of aluminum (x) and basal-plane oxygen (δ) in all the investigated samples are summarized in Table II.

B. Magnetic structure

For all Al-doped single crystals investigated so far AFI ordering sets in below the paramagnetic state. The ground-state AFII phase occurs at low temperatures with components of the AFI and AFII phase coexisting in a limited temperature interval. As an example, the situation is shown for the sample WAX17-1B with $x = 0.19$, δ=0.28. Figure 2 shows the integrated intensity versus temperature for the $(\frac{1}{2},\frac{1}{2},2)$ and $(\frac{1}{2},\frac{1}{2},\frac{3}{2})$ magnetic peaks, which are associated with the AFI and AFII ordering, respectively. The integrated intensity of the $(\frac{1}{2},\frac{1}{2},2)$ magnetic peak shows a power-law behavior $I \sim I_0(T_N - T)^{2\beta}$ with a critical exponent β =0.26(1) fitted between 300 K and T_N. T_N is found to be 407 K. The AFII ordering sets in at $T_2 \approx$17 K. In the temperature range between 6 K and 17 K both the AFI and AFII phases are present indicating competing interactions. The AFI ordering component vanishes completely at temperatures lower than 6 K, while the AFII order parameter saturates.

In order to determine the magnetic structure, several magnetic peaks were investigated at 20 K and 4.2 K for the pure AFI and AFII phase, respectively. The integrated intensities were obtained by fitting the peaks to a Gaussian peak profile. All peaks were resolution-limited

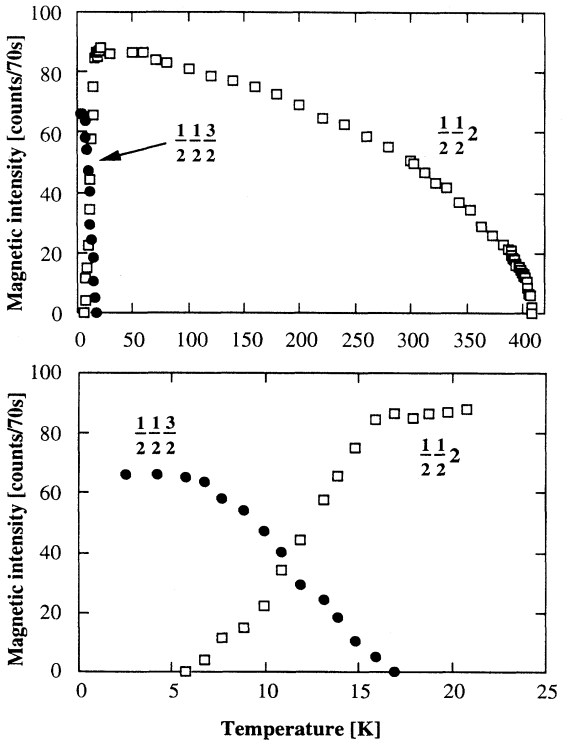

FIG. 2. Integrated intensity vs temperature for the $(\frac{1}{2}\frac{1}{2}2)$ (□) and $(\frac{1}{2}\frac{1}{2}\frac{3}{2})$ (•) magnetic reflections for WAX17-1B. The order parameter $M \sim \sqrt{I}$ shows a power-law behavior $M \sim \mid T - T_N \mid^{\beta}$ with a critical exponent β = 0.26(1) fitted between 300 K and the Néel temperature T_N=407 K. At low temperatures AFII is the stable phase; between 6 K and 17 K both phases coexist.

in h,k as well as in the l direction, which implies that in both phases the spins on Cu lattice sites order long-range and three-dimensionally.

The differential cross section for magnetic scattering is given by[46]

$$\frac{d\sigma_M}{d\Omega}(\vec{\kappa}) = N\frac{(2\pi)^3}{V_0}\sum_{\vec{\tau}} \mid \vec{F}_{M\perp}(\vec{\kappa}) \mid^2 \delta[(\vec{\tau} \pm \vec{Q}) - \vec{\kappa}], \quad (1)$$

where $\vec{\kappa}$ is the scattering vector, $\vec{\tau} = (\frac{2\pi}{a}h, \frac{2\pi}{b}k, \frac{2\pi}{c}l)$ is a crystallographic reciprocal lattice vector with Miller indices (hkl), $\vec{Q} = (\frac{2\pi}{a}q_a, \frac{2\pi}{b}q_b, \frac{2\pi}{c}q_c)$ is the characteristic vector describing the magnetic ordering, $\vec{F}_{M\perp}(\vec{\kappa})$ is the component of the magnetic structure factor perpendicular to $\vec{\kappa}$, N is the number of unit cells, and V_0 the volume of the cell. The square of the magnetic structure factor can be written as

$$\mid \vec{F}_{M\perp}(\vec{\kappa}) \mid^2 = \gamma_0^2\langle 1 - (\hat{\kappa}\cdot\hat{S})^2\rangle f^2(\vec{\kappa})F^2_{\rm geo}(\vec{\kappa})e^{-2W}, \quad (2)$$

where $\gamma_0 = 0.269 \times 10^{-12}$ cm/μ_B is the magnetic scattering length per μ_B, $f(\vec{\kappa})$ is the magnetic form factor for Cu^{2+}, e^{-W} is the Debye-Waller factor, and $F^2_{\rm geo}(\vec{\kappa})$ is defined by Eqs. (5) or (6). The term $\langle 1-(\hat{\kappa}\cdot\hat{S})^2\rangle = \langle \sin^2\alpha\rangle$ is a spin orientation function, which arises from the vectorial magnetic interaction and accounts for the angle α between the spin direction $\vec{S}$ and scattering vector $\vec{\kappa}$. The brackets around $\langle \sin^2\alpha\rangle$ indicate a space and time average over magnetic domains. For our refinements we considered two different spin orientations:

planar model $\vec{S}\perp\vec{c}$: $\langle \sin^2\alpha\rangle = \frac{1}{2}(1 + \cos^2\eta)$,
uniaxial model $\vec{S}\parallel\vec{c}$: $\langle \sin^2\alpha\rangle = \sin^2\eta$,

where $\cos\eta = \frac{\kappa_z}{\kappa}$. In order to take the anisotropy into account we calculated the magnetic form factor using the formulas given by Freeman.[47] For an unpaired $3d_{x^2-y^2}$ electron distribution the aspherical form factor can be written as[3]

$$f(\vec{\kappa}) = \langle j_0\rangle - \frac{5}{7}(1 - 3\cos^2\eta)\langle j_2\rangle + \frac{9}{56}\left(1 - 10\cos^2\eta + \frac{35}{3}\cos^4\eta\right)\langle j_4\rangle. \quad (3)$$

For the $\langle j_n\rangle$ we took the analytical approximations given in the International Tables of Crystallography[48] for Cu^{2+}.

The integrated intensity of magnetic scattering can be written as

$$I(\vec{\kappa}) \sim \frac{d\sigma_M}{d\Omega}(\vec{\kappa})L(\vec{\kappa}), \quad (4)$$

where, in our case, $L(\vec{\kappa})$ is the modified Lorentz factor valid for a step scan with equidistant steps in reciprocal space through a Bragg peak at Bragg angle θ_S. For such a general scan $L(\vec{\kappa})$ may be expressed as $L(\vec{\kappa}) \sim [2\sin\theta_S|\sin(\theta_S - \gamma)|]^{-1}$, where γ is the angle between the scattering vector $\vec{\kappa} = \vec{\kappa}_S$ and the scan direction.[49]

The high-temperature AFI phase gives magnetic reflections which may be indexed as $(h + \frac{1}{2}, k + \frac{1}{2}, l)$ where

TABLE III. Square of the structure factor F^2 of the AFI magnetic Bragg reflections, measured at 20 K and calculated for the two different spin directions (for WAX17-1B).

hkl	κ (Å^{-1})	F^2_{obs} (10^3 b)	F^2_{calc} (10^3 b)	
			$\vec{S} \perp \vec{c}$	$\vec{S} \parallel \vec{c}$
$\frac{1}{2}\frac{1}{2}0$	1.148	< 1	0.0	0.0
$\frac{1}{2}\frac{1}{2}1$	1.266	28.8	28.3	39.4
$\frac{1}{2}\frac{1}{2}2$	1.567	55.8	55.7	40.4
$\frac{1}{2}\frac{1}{2}3$	1.969	14.2	15.0	6.2
$\frac{1}{2}\frac{1}{2}4$	2.423	8.3	7.2	1.8
$\frac{1}{2}\frac{1}{2}5$	2.904	50.4	52.1	9.0
$\frac{1}{2}\frac{1}{2}6$	3.400	40.9	39.5	4.6
$\frac{1}{2}\frac{1}{2}7$	3.907	< 1	1.2	0.1
$\frac{3}{2}\frac{3}{2}1$	3.485	6.8	7.0	13.4
$\frac{3}{2}\frac{3}{2}2$	3.605	12.2	12.4	20.9
$\frac{3}{2}\frac{3}{2}3$	3.798	3.5	3.3	4.6
			$R = 2.8\%$	$R = 60.6\%$
			$\langle S\rangle_{Cu(2)} = 0.58(2)\mu_B$	$\langle S\rangle_{Cu(2)} = 0.56(20)\mu_B$

$l \neq 0$ and h,k,l are integers. The corresponding magnetic cell is doubled in the **a** and **b** directions, i.e., the spins within a single (001) plane show a simple antiferromagnetic arrangement as indicated by the filled and unfilled circles in Fig. 1a. The ordering vector is therefore $\vec{Q}_{AFI} = (\frac{1}{2}\frac{2\pi}{a}, \frac{1}{2}\frac{2\pi}{b}, 0)$, or in reduced reciprocal lattice units: $\vec{q}_{AFI} = (\frac{1}{2}, \frac{1}{2}, 0)$. The extinction rule, that the magnetic reflections with l=0 are absent, further implies that the summation of the ordered moments in the Cu(1) and the two nearest Cu(2) planes is zero, *i.e.*, presumably there is no ordered moment on Cu(1) sites and a perfect antiferromagnetic coupling between ordered moments at Cu(2) sites along **c**, resulting in the stacking sequence $+0-+0-$ along **c**, where 0 belongs to the Cu(1) sites. Considering these symmetry requirements, the geometrical term of the magnetic structure factor normalized to the chemical cell takes the form

$$|F_{geo}(\vec{\kappa})| \sim 2\langle S\rangle_{Cu(2)} \sin(2\pi q_l z), \tag{5}$$

where $\langle S\rangle_{Cu(2)}$ is the mean ordered moment on the Cu(2) site and z is the distance between the Cu(1) and Cu(2) layer in fraction of the unit cell length c. For the single crystal described here (Tables II–IV, Figs. 1–3), we refined a value of $z = 0.3606(2)$.

Table III compares the observed and the calculated magnetic structure factors (as F^2_{obs} and F^2_{calc}) for the two spin directions mentioned above. Nuclear Bragg reflections were used for normalization. The Debye-Waller factor was neglected for the magnetic Bragg peaks. The best agreement between observed and calculated inten-

TABLE IV. Square of the structure factor F^2 of the AFII magnetic Bragg reflections, measured at 4.2 K and calculated for the two different spin directions (for WAX17-1B).

hkl	κ (Å^{-1})	F^2_{obs} (10^3 b)	F^2_{calc} (10^3 b)	
			$\vec{S} \perp \vec{c}$	$\vec{S} \parallel \vec{c}$
$\frac{1}{2}\frac{1}{2}0$	1.148	< 1	0.0	0.0
$\frac{1}{2}\frac{1}{2}\frac{1}{2}$	1.179	7.5	7.6	14.1
$\frac{1}{2}\frac{1}{2}\frac{3}{2}$	1.399	42.0	42.0	42.6
$\frac{1}{2}\frac{1}{2}\frac{5}{2}$	1.760	38.5	37.9	20.9
$\frac{1}{2}\frac{1}{2}\frac{7}{2}$	2.192	< 1	0.1	0.0
$\frac{1}{2}\frac{1}{2}\frac{9}{2}$	2.661	Al powder line	25.7	5.3
$\frac{1}{2}\frac{1}{2}\frac{11}{2}$	3.151	Al powder line	52.3	7.3
$\frac{1}{2}\frac{1}{2}\frac{13}{2}$	3.653	14.1	13.0	1.4
$\frac{3}{2}\frac{3}{2}\frac{1}{2}$	3.454	2.2	2.2	4.4
$\frac{3}{2}\frac{3}{2}\frac{3}{2}$	3.536	9.2	9.7	18.1
$\frac{3}{2}\frac{3}{2}\frac{5}{2}$	3.693	7.9	8.5	12.9
			$R = 2.5\%$	$R = 45.4\%$
			$\langle S\rangle_{Cu(2)} = 0.55(1)\mu_B$	$\langle S\rangle_{Cu(2)} = 0.46(4)\mu_B$
			$\langle S\rangle_{Cu(1)} = -0.03(2)\mu_B$	$\langle S\rangle_{Cu(1)} = 0.09(8)\mu_B$

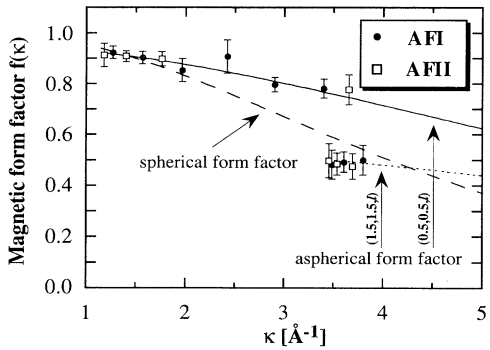

FIG. 3. Comparison between the experimentally deduced form factors $f(\vec{\kappa})$ for Cu^{2+} as a function of $\kappa = 4\pi \sin\theta/\lambda$ with calculated form factors obtained from the spherical or aspherical unpaired $3d_{x^2-y^2}$ electron distributions for WAX17-1B. The different symbols •, □, correspond to the experimental $(h+\frac{1}{2},k+\frac{1}{2},l)$ (AFI) and $(h+\frac{1}{2}, k+\frac{1}{2}, l+\frac{1}{2})$ (AFII), h,k,l integer, reflections, respectively. For the aspherical distribution the solid curve corresponds to the $(\frac{1}{2},\frac{1}{2},l)$ reflections, and the dotted curve to the $(\frac{3}{2},\frac{3}{2},l)$ reflections. The spherical form factor is given by the dashed curve.

sities was obtained with the planar model, which means that the spin direction is lying in the *ab* plane. The averaged moment of the Cu^{2+} ions on the Cu(2) sites was refined to be $0.58(2)\mu_B$. The spin direction as well as the ordered moment on Cu(2) are in good agreement with the results found for the undoped system.[17]

The magnetic peaks at $(h+\frac{1}{2}, k+\frac{1}{2}, l+\frac{1}{2})$, with h,k,l integers, caused by the low-temperature phase AFII belong to a magnetic cell which is doubled along the **a**, **b**, and **c** directions [Fig. 1(b)]. In this case the ordering wave vector is $\vec{Q}_{\mathrm{AFII}} = (\frac{1}{2}\frac{2\pi}{a}, \frac{1}{2}\frac{2\pi}{b}, \frac{1}{2}\frac{2\pi}{c})$, i.e., $\vec{q}_{\mathrm{AFII}} = (\frac{1}{2}\frac{1}{2}\frac{1}{2})$. Thus the ordering within the plane is still antiferromagnetic. The doubling along **c** allows for a possible ordered moment on the Cu(1) lattice sites. Because magnetic reflections with q_l=0 are absent, we find again that the sum of ordered moments along the **c** axis should cancel. Considering these symmetry requirements the two stacking sequences, (i) $++{+}{-}{-}{-}$ and (ii) $+{-}{+}{-}{+}{-}$, along **c** are possible. The geometrical part of the structure factor for the AFII phase normalized to the chemical cell is of the form

$$| F_{\mathrm{geo}}(\vec{\kappa}) | \sim \langle S\rangle_{\mathrm{Cu(1)}} - 2\langle S\rangle_{\mathrm{Cu(2)}} \cos 2\pi q_l z, \qquad (6)$$

where $\langle S\rangle_{\mathrm{Cu(2)}}$ is positive, and $\langle S\rangle_{\mathrm{Cu(1)}}$ is positive for the model with antiferromagnetic orientation of nearest neighbor Cu(1) and Cu(2) sites and negative for ferromagnetic orientation.

Refinements of the models were performed on seven symmetry independent reflections. The results are shown in Table IV. The best agreement between observed and calculated intensities was obtained for a structure with the spin direction lying in the (001) plane. The ordered moment on Cu(2) lattice sites is refined to $0.55(2)\mu_B$ and is thus the same as obtained for the AFI phase. The ordered moment on the Cu(1) lattice site is very small with a value of $-0.03(2)\mu_B$. The negative sign implies a ferromagnetic coupling to the neighboring moments on Cu(2) sites. The stacking sequence along **c** is therefore found to be $+{+}{+}{-}{-}{-}$. The agreement between observed and calculated intensities is only insignificantly different if the Cu(1) moment is set to zero. In other words, our present data do not necessarily prove that there is an ordered moment on Cu(1) sites. Our result for the AFII structure is in agreement with the model proposed by Kadowaki.[10]

Since our Al-doped single crystals show a complete transition from the AFI to the AFII phase, we are able to work out the form factors in each phase and compare them to the calculated form factors. Figure 3 shows such a comparison between the form factors deduced from experiment according to Eq. (2) and the calculated ones for the aspherical unpaired $3d_{x^2-y^2}$ electron distribution given in Eq. (3) as well as for the spherically averaged Cu $3d$ hole. The data of both the AFI phase and the AFII phase demonstrate, that the Cu^{2+} form factor is better described by the aspherical expression than by the spherical approximation, which is obvious since the $x^2 - y^2$ symmetry of the Cu $3d$ orbital is nonspherical.

Table II shows the transition temperatures T_N and T_2 observed for samples with different aluminum and oxygen contents investigated so far. The onset at T_2 of the AFII phase on cooling is not correlated with the Al and O contents in a simple way. The highest T_2 of 18 K in these crystals occurs for an Al content x=0.19 and δ=0.36 and there seems to be the tendency that T_2 increases with x for the same oxygen stoichiometry and sample treatment. In this context it should be noted that the samples WAX17-1C and WAX1-1B were reduced at higher temperatures at a low oxygen partial pressure in order to get the sample as oxygen deficient as possible. Both samples show a strong reduction of T_2, which may be related to the formation of Al-O-Al clusters during the reduction process (see below). For the Al-doped cystals the transition temperature T_N to the paramagnetic state decreases only very slightly with x or δ in the investigated range, but it is significantly depressed in the undoped crystal (WAX28-5) due to the charge transfer related to the rather high oxygen content.

IV. DISCUSSION

Our results show that in Al-doped single crystals, the AFII phase is present at low temperatures. This is in contrast to the undoped system, where this AFII phase is found neither in polycrystalline materials nor in those single crystals, which are definitely very pure (Al-free) and of high quality.[17] The AFI↔AFII transition in our crystals is well defined and significantly sharper than that observed by Kadowaki[10] and Shamato[3] in their samples. Similarly, we observed exceptions from the general tendency that T_2 increases with x for constant δ. The following line of arguments presents a chemical concept, which is consistent with all observations, in particular with the significance of Al doping for the magnetic structure, as well as the relevance of the defect distributions which vary according to the sample treatment.

The refinement of our AFII data favored a structure with a stacking sequence + + + − −−, i.e., a structure with nearest-neighbor Cu(1)-Cu(2) ferromagnetic interactions and nearest neighbor Cu(2)-Cu(2) antiferromagnetic interactions. Thus the formation of the AFII phase is presumably related to the presence of an effective ferromagnetic coupling between Cu(2) ions on next-nearest CuO_2 planes, mediated *via* the intermediate Cu(1) layer. If moments develop on the Cu(1) sites and couple magnetically to the $Cu(2)O_2$ planes, there will be a frustration of the antiferromagnetic arrangement of the Cu(2) spins on the next-nearest-neighboring $Cu(2)O_2$ planes in the AFI phase [Fig. 1(a)]. This frustration is resolved in the AFII structure, which is doubled along the tetragonal **c** axis [Fig. 1(b)]. Consequently, the AFII structure is the ground state when magnetic moments are present in the Cu(1) layer.

The refined ordered moment on Cu(2) lattice sites in the AFII phase is $0.55(1)\mu_B$ and thus very similar to that in the AFI phase. In contrast the refined *ordered* moment on the Cu(1) sites is only $-0.03(2)\mu_B$ and hardly significant. From mean field calculations,[50] a moment of $1.1\mu_B$ is expected for Cu^{2+}. The reduction of the Cu^{2+} moment to about one half of this theoretical value can be explained by quantum fluctuations resulting from the $2d$ character of the spin wave spectrum[50] and the covalency of the orbital of the Cu(2) with the neighboring oxygen orbitals.[51] It is clear that the ordered magnetic moment on Cu(1) sites should be much smaller than that on the Cu(2) site, because only a part of the Cu(1) is formally oxidized from Cu^{1+} to Cu^{2+} by the residual oxygen in the basal plane. The disordered oxygen and aluminum distribution in the Cu(1) layer, however, makes it quite difficult to estimate the amount of Cu^{2+} ions on the Cu(1) lattice sites for a given oxygen and aluminum content. Assuming simply that each aluminum attracts one excess oxygen and that the remaining oxygens each oxidize their two Cu(1) neighbors to Cu^{2+}, the fraction of Cu^{2+} in the basal plane would be $2(\delta - x)$. Hence, for a sample with δ=0.28 and x=0.19 one may expect a fraction of 0.18 Cu^{2+} in the basal plane. A local moment of about $0.5\mu_B$ per Cu^{2+} could thus lead to an average ordered moment $\langle S\rangle_{Cu(1)}$ on the Cu(1) lattice site of roughly $0.1\mu_B$. Our refined ordered moment on the Cu(1) site is still a factor of 3 smaller and practically zero within the limits of error. This is supported by NQR measurements[36] which show that Cu—O—Cu chain fragments are present in the Cu(1) plane, which carry no magnetic moment. We expect that in the case of a clustered Al distribution [Fig. 4(a)] no magnetic moments will be present: it is obvious that there is no magnetic moment in the type of Al-O-Al clusters shown in Fig. 4(a), while the spins on the Cu^{2+} ions in isolated Cu^{2+}–O^{2-}–Cu^{2+} "chain fragments" most likely will form singlet pairs with essentially no net magnetic moment [cf. Fig. 4(a)]. In the contrasting case of a random Al distribution, moments most likely will form on Cu^{2+} ions that are part of the Al^{3+}—O^{2-}—Cu^{2+} shown in Fig. 4(b), because these Cu^{2+} ions are weakly coupled to one another. Thus, with significant Al clustering and low oxygen content ($\delta \approx x$) there will be essentially no magnetic moment

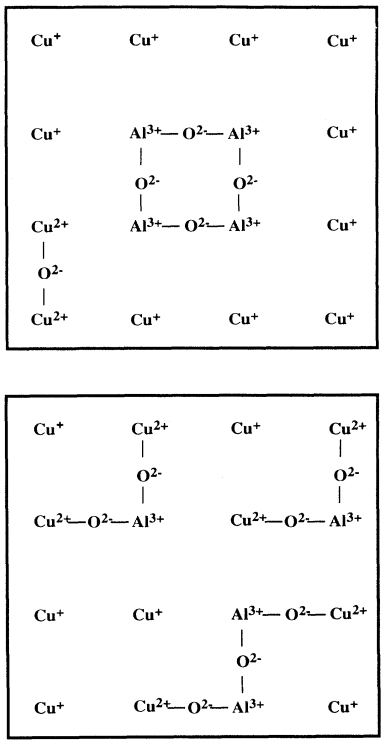

FIG. 4. Chain fragments in samples with (a) clustered and (b) random Al distribution. Homogeneous Al^{3+}—O^{2-}—Al^{3+} and Cu^{2+}—O^{2-}—Cu^{2+} chain fragments are nonmagnetic (the latter will form a singlet state), whereas heterogeneous Cu^{2+}—O^{2-}—Al^{3+} chain fragments carry magnetic moments on the Cu^{2+} sites.

in the Cu(1) chain structure [Fig. 4(a)], whereas a random Al distribution with excess oxygen ($\delta > x$) will give rise to islands with free Cu^{2+} spins, which may trigger the formation of the AFII phase [Fig. 4(b)]. Therefore the Al-O cluster configuration will have a significant influence on the stability of the AFII phase *via* the control of the local magnetic structure in the Cu(1) "chain" layer. That this is indeed the case has been shown recently by Uimin and Andersen.[52] Recalling that experimental[25,27–29,30] and computer simulation studies[53] have shown significant clustering of Al, Co, and Fe ions in YBaCuO if the material is reduced at high temperature, we believe that the lack of clear correlations between the oxygen and aluminum content and the observed transition temperature T_2 to the antiferromagnetic AFII phase is a consequence of the details of the crystal treatment. This is consistent with our recent experimental structural studies of Al-doped YBaCuO which have shown that the threshold temperature for significant clustering to occur in a reducing atmosphere is 973 K, which is within the temperature range used in the present sample preparations (cf. Table II).[30]

The limited temperature interval below T_2 in which magnetic peaks with q_c=0 and q_c=1/2 coexist may be interpreted in two ways, which cannot be distinguished by the present diffraction data. The phase transition may be of first order in which case domains with the

collinear AFI and AFII structures may coexist. On the other hand, a second-order transition between the two structures may be established by a continuous antiphase rotation of the Cu(2) spins in next-nearest-neighboring CuO_2 planes as pointed out by Kadowaki.[10] As shown in Fig. 5 the AFI structure with $\beta=0°$ is transformed into the AFII structure for a rotation angle of $\beta=90°$. For intermediate angles a separate noncollinear magnetic structure exists [Fig. 5(c)], which gives rise to both sets of magnetic Bragg peaks. In any case, the intermediate ordered state is caused by competing interactions between nearest and next-nearest Cu sites. Furthermore, the local magnetic structure, which may include domains of three distinct phases, will be strongly effected by the distribution and ordering field strength of magnetic islands in the Cu(1) chain structure.

A full realization of the mechanisms and the structural configurations that give rise to the AFII phase has not yet been established. In the recent work of Casalta *et al.*[17] the significance of the Al was demonstrated in the sense that for two high-purity samples with an oxygen content $\delta=0.1$ and 0.18 this phase was not observed. This observation has been corroborated further in the present work where an undoped single crystal was reduced in a controlled way[43] to obtain $\delta=0.25$, which is comparable to the oxygen content of the Al-doped WAX1-1A single crystal (cf. Table II). From the refinement of the nuclear Bragg reflection data set, an oxygen content of $\delta=0.23$ in the basal plane was obtained. In the WAX28-5 single crystal no AFII phase was observed whereas the WAX1-1A with $x=0.14$ has $T_2=8$ K.

Comparing our results on Al-doped crystals with those for Co- and Fe-doped materials, we find a similar behavior at a low doping levels, whereas the effects are completely different at higher doping levels. Miceli *et al.*[31,32] performed studies on polycrystalline samples with a Co content of 0.20 in the Cu(1) plane, which is comparable to the highest amount of Al in the samples we investigated.

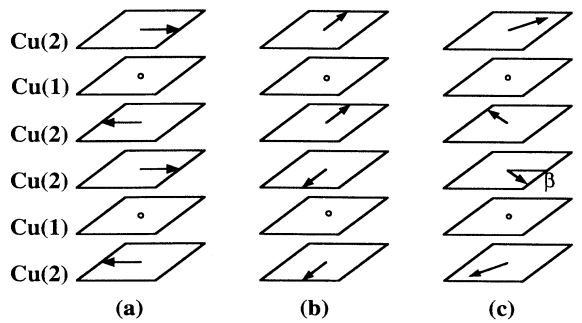

FIG. 5. Stacking of the spins along the **c** axis of the AFI (a) and AFII (b) phase. The moments in the collinear AFI are assumed to be perpendicular to the moments in the collinear AFII phases. The resultant spin structure of the hypothetical noncollinear intermediate phase AFI∩ AFII according to the spin rotation model (c) results from a vector summation of the two collinear structures (a) and (b) leading to the canting angle β. Note that the spins rotate in the same sense within a $Cu(2)O_2$ double layer, while the sense of rotation alternates across the Cu(1) position from double layer to double layer.

The authors report that T_2 is strongly affected by the oxygen content. For an oxygen content of about 6.3 only the AFII phase is observed with a T_N of about 400 K, which rapidly drops with increasing oxygen content. At a higher Co content the AFII phase seems to be stabilized, also at high oxygen content. Zolliker *et al.*[26] found in $YBa_2Cu_{2.16}Co_{0.84}O_{7.32}$ ceramics only AFII ordering, but they claim that the moment direction is parallel to the **c** axis. Based on our data this spin direction must be ruled out for Al-doped materials. In reduced Fe-substituted ceramic material it was reported from neutron scattering[34] and from Mössbauer[37] investigations that for low Fe content the AFII phase is stable at low temperatures only [$T_2 \approx 50$ K,[34] $T_2 \approx 25$ K (Ref. 37)] and the AFI phase exists up to $T_N \approx 400$ K, while at a certain threshold value of x [$x_t=0.06$,[34] $x_t=0.24$ (Ref. 37)] the AFII ordering exists over the whole antiferromagnetically ordered regime up to T_N. The discrepancies in T_2 and x_t may also be explained by a different Fe-cluster formation due to a different reduction process. Considering the magnetic moment of Fe^{2+}/Fe^{3+}, the magnetic transition temperatures may be more sensitive to clustering than in the case of Al doping. The observation of a small field on the Cu(1) lattice sites was also reported by Lütgemeier *et al.*[36] in NQR studies of Al- and Fe-doped ceramic material, where the Cu(1) line shows the typical Zeeman splitting. Therefore it seems that the Al-doped system shows the same properties as the Fe- and Co-doped system at low doping levels, indicating that the defect ions only act as an impurity. At a higher doping level the magnetic properties of Fe and Co become important, stabilizing the AFII structure, whereas the nonmagnetic Al still acts only as an impurity at higher substitution.

In contrast to our results, Miceli *et al.*[54] did not observe any AFII phase in Al-doped ceramic samples, neither at low nor at high doping levels. Furthermore, the T_N value of $T_N \approx 500$ K for an Al-doped sample with $x = 0.1$ reported by this group is unusually high. Kumagai *et al.*[55] found no evidence for AFII ordering in NMR studies of polycrystalline Al-doped samples.

As a summary, Fig. 6 shows all the magnetic transitions discussed so far for these materials: in the oxygen deficient, undoped $YBa_2Cu_3O_{6+\delta}$ materials, the transition from the paramagnetic to the antiferromagnetic AFI phase occurs near $T_N=400$ K. In highly Fe- and Co-doped material the magnetic character of the dopant induces a field, which is sufficiently strong to induce a transition from the paramagnetic phase directly into the AFII ground state phase. In the Al-doped and the Fe- and Co-doped systems at low concentration, the magnetic centers in the Cu(1) layer are diluted, and the strength of the resulting noncoherent defect field is too weak to stabilize the AFII ordering at high temperatures. At $T_N \approx 400$ K the transition to the AFI phase occurs, whereas at low temperatures a reordering to the AFII phase as the ground state phase can be observed. Reordering between AFI and AFII can take place either via a direct first-order transition with phase coexistence, or as a continuous one via two second-order phase transitions with an intermediate phase AFI∩AFII. The symmetry of the latter phase is a combination of the sym-

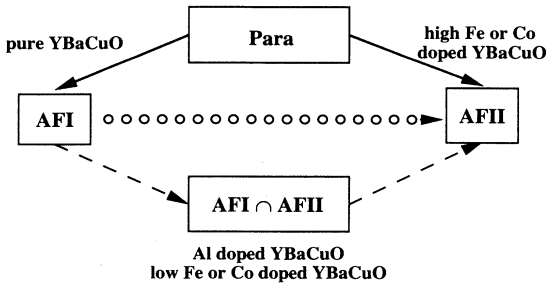

FIG. 6. Schematic representation of the observed magnetic phase transitions. The arrows point in the direction of decreasing temperature. The direct transition between the paramagnetic phase and AFI is found in the pure system, the Al-doped system and the Fe- and Co-doped systems at low doping levels. In the highly doped Fe, Co system, the AFII phase reaches up to the paramagnetic state. Reordering between AFI and AFII can take place either via a direct first order transition (with defect-induced phase coexistence) or via two second-order phase transitions via an intermediate phase AFI∩AFII.

metry elements of the AFI and AFII phase. From the present neutron-diffraction data we are not able to distinguish between these two possibilities. Kadowaki *et al.*[10] and more recently Mirebeau *et al.*[56] preferred the spin rotation model from the energetical point of view and the fact that no hysteresis in the AFI↔AFII transition is observed. NQR experiments on Al-doped single crystals, which will be reported elsewhere[57] support the spin rotation model.

V. CONCLUDING SUMMARY

Our results show that Al induces the transition from the AFI to the AFII structure at low temperatures. We believe that this transition is driven by the defect field of magnetic moments introduced in the Cu(1) layer, as these moments are frustrated in the AFI structure. Since this AFI↔AFII transition is not observed in pure YBaCuO with various oxygen contents, the magnetic reordering cannot be explained alone by the oxygen in the chain layers creating moments on Cu(1) lattice sites. However, the Al defect ions may develop free Cu spins at Al—O—Cu chain fragments as shown in Fig. 4(b), which may give rise to the transition to the AFII structure at low temperatures. This feature is similar to the effects caused by doping with Fe and Co at a low doping level. At higher doping levels, in the Fe- and Co-doped systems the magnetic nature of the dopant becomes dominant destroying the AFI phase and stabilizing the AFII phase. In this context, studies of the magnetic structure in the mixed AFI/AFII region are of significant interest, and they will be conducted. Furthermore, we have shown that the Al distribution and thus the thermal treatments are also important for the magnetic effects in these materials, which may explain the large discrepancies concerning the AFI↔AFII transition in the literature. In order to get a clearer picture it is important to consider the synthesis procedures and heat treatments for each sample to be compared in detail.

ACKNOWLEDGMENTS

We gratefully acknowledge H. Lütgemeier and S. Schmenn for reading the manuscript and fruitful discussions. Stimulating discussions with G. Uimin are also greatly acknowledged. E.B. thanks J. Lebech, M. Lund, F. Saxild, and B. Breiting for their technical assistance. Part of this work is supported by the Danish Ministry of Energy and the CEC Science and Esprit program. The neutron scattering experiments reported in this paper were performed at the DR3 reactor at Risø National Laboratory and supported by the Commission of the European Community through the Large Installation Plan. E.B. and W.W.S. gratefully acknowledge the Deutsche Forschungsgemeinschaft (DFG) for financial support.

[1] N. Nishida, Jpn. J. Appl. Phys. **26**, L1856 (1987).
[2] J. M. Tranquada, D. E. Cox, W. J. Kunnmann, H. Moudden, M. Suenaga, P. Zolliker, D. Vaknin, S. K. Sinha, M. S. Alvarez, A. J. Jacobson, and D. C. Johnston, Phys. Rev. Lett. **60**, 156 (1988).
[3] S. Shamato, M. Sato, J. M. Tranquada, B. J. Sternlieb, and G. Shirane, Phys. Rev. B **48**, 13 817 (1993).
[4] J. M. Tranquada, A. H. Moudden, A. I. Goldman, P. Zolliker, D. E. Cox, G. Shirane, S. K. Sinha, D. Vaknin, D. C. Johnston, M. S. Alvarez, A. J. Jacobson, J. T. Lewandowski, and J. M. Newsam, Phys. Rev. B **38**, 2477 (1988).
[5] J. H. Brewer, E. J. Ansaldo, J. F. Carolan, A. C. D. Chaklader, W. N. Hardy, D. R. Harshman, M. E. Hayden, M. Ishikawa, N. Kaplan, R. Keitel, J. Kempton, R. F. Kiefl, W. J. Kossler, S. R. Kreitzman, A. Kulpa, Y. Kuno, G. M. Luke, H. Miyatake, K. Nagamine, Y. Nakazawa, N. Nishida, K. Nishiyama, S. Ohkuma, T. M. Riseman, G. Roehmer, P. Schleger, D. Shimada, C. E. Stronach, T. Takabatake, Y. J. Uemura, Y. Watanabe, D. L. Williams, T. Yamazaki, and B. Yang, Phys Rev. Lett. **60**, 1073 (1988).
[6] P. Burlet, C. Vettier, M. J. G. M. Jurgens, J. Y. Henry, J. Rossat-Mignod, H. Noel, M. Potel, P. Gougeon, and J. C. Levet, Physica C **153-155**, 1115 (1988).
[7] M. J. Jurgens, P. Burlet, C. Vettier, L. P. Regnault, J. Y. Henry, J. Rossat-Mignod, H. Noel, P. Gougeon, and J. C. Levet, Physica B **156-157**, 846 (1989).
[8] J. Rossat-Mignod, P. Burlet, M. J. Jurgens, C. Vettier, L. P. Regnault, J. Y. Henry, C. Ayache, L. Foro, H. Noel, M. Potel, P. Gougeon, and J. C. Levet, J. Phys. (Paris) Colloq. **49**, C8-2119 (1988).
[9] D. Petitgrand and G. Collin, Physica C **153-155**, 1922 (1988).
[10] H. Kadowaki, M. Nishi, Y. Yamada, H. Takeya, H. Takei, S. M. Shapiro, and G. Shirane, Phys. Rev. B **37**, 7932 (1988).

[11] A. H. Moudden, G. Shirane, J. M. Tranquada, R.J. Birgeneau, Y. Endoh, K. Yamada, Y. Hidaki, and T. Murakami, Phys. Rev. B **38**, 8720 (1988).
[12] J. W. Lynn, W. H. Li, H. A. Mook, B. C. Sales, and Z. Fisk, Phys. Rev. Lett. **60**, 2781 (1988).
[13] K. Zhang, B. Dabrowski, C. U. Segre, D. G. Hinks, I. K. Schuller, J. D. Jorgensen, and M. Slaski, J. Phys. C **20**, L935 (1987).
[14] S. Li, E. A. Hayri, K. V. Ramanujachary, and M. Greenblatt, Phys. Rev. B **38**, 2450 (1988).
[15] T. Iwata, Y. Tajima, and M. Hikita, J. Cryst. Growth **91**, 274 (1988).
[16] S. Katsuyama, H. Izumida, K. Majima, and H. Nagai, Physica C **222**, 317 (1994).
[17] H. Casalta, P. Schleger, E. Brecht, W. Montfrooij, N. H. Andersen, B. Lebech, W. W. Schmahl, H. Fuess, Ruixing Liang, W. N. Hardy, and Th. Wolf, Phys. Rev. B **50**, 9688 (1994).
[18] J. M. Tarascon, P. Barboux, P. F. Miceli, L. H. Greene, G. W. Hull, M. Eibschutz, and S. A. Sunshine, Phys. Rev. B **37**, 7458 (1988).
[19] Y. Xu, M. Suenaga, J. Tafto, R. L. Sabatini, and A. R. Moodenbaugh, Phys. Rev. B. **39**, 6667 (1989).
[20] W. W. Schmahl, A. Putnis, E. Salje, P. Freeman, A. Graeme Barber, R. Jones, K. K. Singh, J. Blunt, P. P. Edwards, J. Loram, and K. Mirza, Philos. Mag. Lett. **60**, 241 (1989).
[21] F. Bridges, J. B. Boyce, T. Claeson, T. H. Geballe, and J. M. Tarascon, Phys. Rev. B **39**, 11 603 (1989).
[22] J. F. Bringley, T. M. Chen, B. A. Averill, K. M. Wong, and S. J. Poon, Phys. Rev. B **38**, 2432 (1988).
[23] G. Kallias, V. Psyharis, D. Niarchos, and M. Pissas, Physica C **174**, 316 (1991).
[24] Y. Ren, W. W. Schmahl, E. Brecht, and H. Fuess, Physica C **199**, 414 (1992).
[25] S. Katsuyama, Y. Ueda, and K. Kosuge, Physica C **165**, 404 (1990).
[26] P. Zolliker, D. E. Cox, J. M. Tranquada, and G. Shirane, Phys. Rev. B **38**, 6575 (1988).
[27] M. G. Smith, R. D. Taylor, and H. Oesterreicher, Phys. Rev. B **42**, 4202 (1990).
[28] A. R. Moodenbaugh, C. Y. Yang, Y. Zhu, R. L. Sabatini, D. A. Fischer, Y. Xu, and M. Suenaga, Phys. Rev. B **44**, 6991 (1991).
[29] H. Renevier, J. L. Hodeau, T. Fournier, P. Strobel, M. Marezio, J. C. Martinez, and J. J. Prejean, J. Less-Common Matter **164-165**, 907 (1990).
[30] E. Brecht, W. W. Schmahl, G. Miehe, H. Fuess, N. H. Andersen, and Th. Wolf, Physica C **235-240**, 471 (1994).
[31] P. F. Miceli, J. M. Tarascon, L. H. Greene, P. Barboux, M. Giroud, D. A. Neumann, J. J. Rhyne, L. F. Schneemeyer, and J. V. Waszczak, Phys. Rev. B **38**, 9209 (1988).
[32] P. F. Miceli, J. M. Tarascon, P. Barboux, L. H. Greene, B. G. Bagley, G. W. Hull, M. Giroud, J. J. Rhyne, and D. A. Neumann, Phys. Rev. B **39**, 12 375 (1989).
[33] J. L. Garcia-Munoz, J. Rodriguez-Carvajal, S. H. Kilcoyne, C. J. Boardman, and R. Cywinski, J. Magn. Magn. Mater. **104-107**, 555 (1992).
[34] I. Mirebeau, C. Bellouard, M. Hennion, V. Caignaert, and E. Suard, J. Appl. Phys. **73**, 5689 (1993).
[35] I. Mirebeau, C. Bellouard, M. Hennion, G. Jehanno, V. Caignaert, A. J. Dianoux, T. E. Philipps, and K. Moorjani, Physica C **184**, 299 (1991).
[36] H. Lütgemeier and B. Rupp, J. Phys. (Paris) Colloq. **49**, C8-2147 (1988); R. A. Brand, Ch. Sauer, H. Lütgemeier, and P. M. Meufels, Hyperfine Interact. **55**, 1229 (1990); H. Lütgemeier and I. Heinmaa, in *Proceedings of XXVI Zakopane School on Physics*, Zakopane, 1991, edited by J. Stanek and A. T. Pedziwiatr (World Scientific, Singapore, 1991), p. 264.
[37] I. S. Lyubutin, V. G. Terziev, S. V. Luchko, A. Ya. Shapiro, A. M. Balagurov, and G. A. Bonch Osmolovskiy, Physica C **199**, 296 (1992); I. S. Lyubutin, V. G. Terziew, T. V. Dmitrieva, S. V. Luchko, and A. Ya. Shapiro, Solid State Commun. **86**, 651 (1993).
[38] D. Hechel, I. Nowik, E. R. Bauminger, and I. Felner, Phys. Rev. B **42**, 2166 (1990).
[39] Th. Wolf, W. Goldacker, B. Obst, G. Roth, and R. Flükiger, J. Cryst. Growth **96**, 1010 (1989).
[40] J. Geerk, G. Linker, and O. Meyer, Mater. Sci. Rep. **4**, 195 (1989).
[41] N. H. Andersen, B. Lebech, and H. F. Poulsen, Physica C **172**, 31 (1990).
[42] P. Schleger, W. N. Hardy, and B. X. Yang, Physica C **176**, 261 (1991).
[43] P. Strobel, J. J. Capponi, M. Marezio, and P. Monod, Solid State Commun. **64**, 513 (1987).
[44] G. M. Sheldrick, SHELX76, Program for crystal structure determination, University of Cambridge, England, 1976.
[45] E. Brecht, W. W. Schmahl, G. Miehe, H. Fuess, N. H. Andersen, J. Hanssmann, and Th. Wolf (unpublished).
[46] J. Rossat-Mignod, in *Methods of Experimental Physics, Neutron Scattering*, edited by K. Sköld and D. L. Price (Academic Press, New York, 1987), p. 69.
[47] A. J. Freeman, Acta Crystallogr. **12**, 261 (1959); Phys. Rev. **113**, 169 (1959).
[48] *International Tables for X-Ray Crystallography*, edited by A. J. C. Wilson (Kluwer Academic Press, Dordrecht, 1992), Vol. C.
[49] B. Lebech and M. Nielsen (unpublished).
[50] J. Rossat-Mignod, L. P. Regnault, C. Vettier, P. Burlet, J. Y. Henry, and G. Lapertot, Physica B **169**, 58 (1991).
[51] T. A. Kaplan, S. D. Mahanti, and Hyunju Chang, Phys. Rev. B **45**, 2565 (1992).
[52] G. Uimin and N. H. Andersen (unpublished).
[53] S. Mannsteadt, T. Fiig, N. H. Andersen, P.-A. Lindgård, and O. G. Mouritsen, Comput. Mater. Sci. **3**, 9 (1994).
[54] P. F. Miceli, J. M. Tarascon, L. H. Greene, J. J. Rhyne, and D. A. Neumann, Physica C **162-164**, 1267 (1989).
[55] K. Kumagai, T. Takatsuka, and A. Yammaka, J. Magn. Magn. Mater. **104-107**, 577 (1992).
[56] I. Mirebeau, E. Suard, V. Caignaert, and B. Bourée, Phys. Rev. B **50**, 3230 (1994).
[57] E. Brecht and S. Schmenn *et al.* (unpublished).